Role of molecular electronic structure in inelastic electron tunneling spectroscopy: O_2 on Ag(110)

Serge Monturet,[1] Maite Alducin,[2,3] and Nicolás Lorente[4]
[1]*Institut für Chemie, Universität Potsdam, Karl-Liebknecht-Straße 24-25, D-14476 Potsdam-Golm, Germany*
[2]*Centro de Física de Materiales, Materials Physics Center (MPC), CSIC-UPV/EHU, P. Manuel de Lardizabal 5, 20018 San Sebastián, Spain*
[3]*Donostia International Physics Center (DIPC), P. Manuel de Lardizabal 4, 20018 San Sebastián, Spain*
[4]*Centre d'Investigació en Nanociència i Nanotecnologia, CSIC-ICN, E-08193 Bellaterra, Spain*
(Received 8 June 2010; revised manuscript received 22 July 2010; published 31 August 2010)

Density-functional theory (DFT) simulations corrected by the intramolecular Coulomb repulsion U are performed to evaluate the vibrational inelastic electron tunneling spectroscopy (IETS) of O_2 on Ag(110). In contrast to DFT calculations that predict a spinless adsorbed molecule, the inclusion of the U correction leads to the polarization of the molecule by shifting a spin-polarized molecular orbital toward the Fermi level. Hence, DFT+U characterizes O_2 on Ag(110) as a mixed-valent system. This has an important implication in IETS because a molecular resonance at the Fermi level can imply a decrease in conductance while in the off-resonance case, an increase in conductance is the expected IETS signal. We use the lowest-order expansion on the electron-vibration coupling in order to evaluate the magnitude and spatial distribution of the inelastic signal. The final IET spectra are evaluated with the help of the self-consistent Born approximation and the effect of temperature and modulation-voltage broadening are explored. Our simulations reproduce the experimental data of O_2 on Ag(110) [J. R. Hahn, H. J. Lee, and W. Ho, Phys. Rev. Lett. **85**, 1914 (2000)] and give extra insight of the electronic and vibrational symmetries at play. This ensemble of results reveals that the IETS of O_2 is more complicated that a simple decrease in conductance and cannot be ascribed to the effect of a single molecular-orbital resonance.

DOI: 10.1103/PhysRevB.82.085447 PACS number(s): 68.37.−d, 72.10.−d, 72.25.−b, 79.20.Rf

I. INTRODUCTION

Single-molecule vibrational spectroscopy is now possible thanks to the development of the inelastic electron tunneling spectroscopy (IETS) operating with the scanning tunneling microscope (STM).[1] The STM is thus conferred with the ability to chemically analyze surfaces on the atomic scale.[2,3] IETS has rapidly become a mature technique and multimode analyses on molecular substrates have been accomplished[4] as well as analyses of extended vibrations or phonons.[5] The characterization and control of single-molecule reactivity through the excitation of a specific vibrational mode is a challenging area for the STM-based IETS technique.[6,7] Within this context, the interaction of O_2 with metals, which plays a central role in many technological processes, has served as a model system to explore and control the fundamentals of gas/surface reactivity.

The chemisorption and dissociation of O_2 on silver surfaces have been widely investigated in last decades in an attempt to understand the catalytic properties of silver, which are extensively exploited in industrial-oxidation processes. Molecular-beam experiments provide detailed information on how reactivity depends on the collision energy, the molecular rovibrational or electronic state, and the surface temperature and coverage. Combining this technique with either electron-energy-loss spectroscopy (EELS), infrared spectroscopy, or thermal desorption spectroscopy (TDS), it is also possible to extract information on the energetics ruling the elementary gas/surface processes—activation energies, atomic and molecular adsorption energies, and reactive paths. Thanks to these kind of studies we know that O_2 dissociation on flat Ag surfaces is characterized by rather large activation energies[8,9] and, as a consequence only molecular adsorption is possible at crystal temperatures below 150 K.[10–12] The chemisorption of O_2 on the Ag(110) surface has been particularly controversial because of the initial disagreement regarding the nature and orientation of the chemisorbed molecule. Density-functional calculations performed by Gravil *et al.*[8] shed light on this controversy showing the existence of two distinct chemisorption states with essentially equal energies. This theoretical finding was subsequently corroborated by EELS and TDS studies,[13] though the final confirmation came with the STM-IETS investigations by Hahn *et al.*[14–16] Compared with other spectroscopies, the great advantage of IETS operated with STM is that it provides simultaneous topographical and spectroscopical images with atomic resolution. This permits an almost *direct* identification of the molecular state.

Molecular O_2 chemisorbs on Ag(110) parallel to the surface over the hollow site on two possible configurations, one with the molecular axis along the [001] surface direction (O_2[001]) and the other one along the [1$\bar{1}$0] direction (O_2[1$\bar{1}$0]). With STM-IETS, single-molecule vibrations are detected with STM-IETS on the O_2[001] only. The recorded inelastic signal is a *decrease* in conductance for one of the modes (the O-O stretch) and it can be a *decrease* or an *increase* in conductance depending on the position of the STM tip over the molecule for the other detected mode (the antisymmetric O_2-Ag stretch).[14] The reasons behind this rich and complex IETS structure have been a matter of controversy that have recently been solved.[17]

In IETS, the changes in conductance are recorded as a function of the tip-substrate voltage. It is generally admitted that in tunneling, the excitation of a vibration mode leads to

opening an inelastic channel for conduction, hence increasing the conductance.[18–21] However, early model calculations predicted that when a molecular resonance overlaps the Fermi level of the substrate, IETS could also give rise to decreases in conductance.[18] Up to now, the $O_2[001]$ is the only example, where such decreases in conductance have been observed experimentally. Strikingly, state-of-the-art IETS simulations, which use the electronic-structure calculated with density-functional theory (DFT) as the initial ingredient, have been unable to reproduce the experimental conductance decreases. The simulations give conductance increases because in the DFT electronic structure the π_g orbitals are not on resonance with the Fermi level.[20,22] This discrepancy led to speculate that the theoretical Fermi level was wrongly positioned. However, questioning the position of the Fermi level and, thus, the molecular charge state in this system is at variance with the excellent characterization of the two experimental chemisorption states given by DFT.[8] Moreover, the Fermi-level fitting,[20,22] thought to force the π_g resonance, cannot reproduce the rich IETS structure of the experimental data showing increases and decreases according to the vibrational mode and the tip localization.

In a recent letter,[17] it has been shown that correcting the DFT electronic structure to adequately incorporate the on-site Coulomb repulsion (the so-called DFT+U approach), the experimental conductance changes recorded over the O-O stretch mode and the antisymmetric O_2-Ag mode are correctly reproduced. Furthermore, the DFT+U calculations permit us to gain extra insight on the actual electronic structure of this molecular system. Contrary to the previous speculations, rather than shifting toward the Fermi level, the π_g resonance follows a Stoner-type splitting of its spin components, leading to the partial filling of one of the spin components of the π_g orbitals and, thus, to the spin polarization of a single O_2 molecule on Ag (110). In the present contribution we present a comparative analysis of the DFT+U electronic structure of the $O_2[001]$ and $O_2[1\bar{1}0]$ states, discussing the properties that cause the respective survival and quenching of the intrinsic O_2 paramagnetism. Indeed, the final electronic structure of $O_2[1\bar{1}0]$ corresponds to a mixed-valent one, where the molecular spin is quenched by rapid charge fluctuations with the metal substrate.[23] Our previous simulations[17] of the conductance changes for the $O_2[001]$ state are extended to all the relevant molecule-surface modes and also to the $O_2[1\bar{1}0]$ molecule. In particular, the reasons for the existence or absence of IETS signal are explained in terms of the electronic and vibrational mode symmetries. There are two symmetry planes in the O_2/Ag(110) system. We show that the possibility to excite a vibrational mode is determined by the overall symmetry character of the coupling states and mode respect to those two planes. However, the value of the IETS signal depends ultimately on the energies of the orbitals and on the strength of the electron vibration coupling. Also, we evaluate the IETS spectra with the help of the self-consistent Born approximation (SCBA) and explore the effects due to temperature and modulation-voltage broadening.

The reminder of the paper is organized as follows. Section II A describes the details of the DFT+U calculations performed to obtain the electronic spectra of O_2 chemisorbed on Ag(110). In Sec. II B, we discuss the necessity to go beyond the harmonic approximation in order to obtain accurate vibrational frequencies of the molecule-surface modes. The theoretical model used for the IETS simulations is explained in Sec. II C. The calculated electronic structure is shown in Sec. III. The corresponding STM-IETS simulations are discussed in Sec. IV. In Sec. V, we apply the SCBA model to calculate the IETS. Conclusions and final remarks are presented in Sec. VI.

II. METHODS

A. Details of the DFT+U calculations

Density-functional theory calculations are performed with the VASP code[24] using plane waves with an energy cutoff of 515 eV and the projector augmented wave method.[25] We use a periodic supercell consisting of a six-layer slab separated by 10.45 Å of vacuum and a (3×4) surface unit cell large enough to significantly reduce interactions among oxygen molecules in neighboring cells. The surface Brillouin zone is sampled with a $4\times4\times1$ Monkhorst-Pack grid of special k points. The exchange and correlation energy is calculated within generalized gradient approximation (GGA) using the PW91 functional.[26] The calculations are stopped when the total energy changes less than 1×10^{-5} eV and the forces on ions are below 0.02 eV/Å. The chemisorption energy of the two configurations computed here are 0.439 eV for the $O_2[001]$ and 0.449 $O_2[1\bar{1}0]$. Despite the small energy difference between configurations the actual barrier is in the range of 400 meV.[8,16] Corrections to the on-site Coulomb repulsion are applied to the oxygen $2p$ electrons following the rotationally invariant DFT+U scheme proposed by Dudarev *et al.*[27] as implemented in VASP. The screened on-site Coulomb interaction U is calculated from first principles as the energy cost for adding extra charge to O_2 when adsorbed on Ag(110). The value obtained with the method described in Ref. 28 is close to 4 eV. However, we also verify that the results shown in this work are reproduced for U varying within the range 2–4 eV. Such a verification is necessary because the calculated U value actually depends on the projectors and the used constrained method to fix the final electronic structure. The adsorption positions are optimized by fully relaxing the O atoms and the two uppermost silver layers until atomic forces are less than 0.02 eV/Å.

B. Vibrational frequency evaluation: Beyond the harmonic approximation

The diagonalization of the dynamical matrix gives the vibrational modes within the harmonic approximation. The method implemented in VASP uses finite differences to compute the second derivative of the Hamiltonian with respect to a constant displacement ΔR of every coordinate of the active atoms, here the oxygen ones. In Table I we report the vibrational energies of the first four (more energetic) $O_2[001]$ molecular modes for atomic displacements, $\Delta R=0.02$ and 0.04 Å. The GGA+U calculation with a displacement of 0.04 Å is the one that has the better overall agreement with

TABLE I. Semilocal DFT (GGA) and DFT+U (GGA+U with U=3 eV) vibrational mode energies (meV) of O_2[001]. The value ΔR is the displacement of the oxygen atomic coordinates used in each case to evaluate the dynamical matrix. The modes are schematically depicted in Fig. 5.

	ΔR=0.02 Å		ΔR=0.04 Å		
Mode	GGA	GGA+U	GGA	GGA+U	Experiment
O-O stretch	92.9	92.4	96.1	90.1	82.0,[a]85.0[b]
Antisym. O_2-Ag	47.3	49.3	29.2	33.2	38.3[a]
Center of mass	43.9	43.5	19.0	24.6	30[c,d]
Hindered rotation	39.0	33.8	38.2	34.5	

[a]Reference 14.
[b]Reference 13.
[c]Reference 29.
[d]Reference 30.

the experimental measurements. The dispersion is still considerable, despite the fact that DFT is known to yield frequencies within ~5% of the experimental values.[31] The harmonic approximation seems to be inadequate to capture the complexity of the molecular modes in this system and, in particular, of the softer modes, whose energies strongly fluctuate with ΔR. Indeed, we observe that some matrix elements, which correspond to the smallest values of the second derivatives, lead to an asymmetric dynamical matrix. To confirm the anharmonicity of the problem, we have performed a more exhaustive calculation of the normal modes.

For each vibrational mode, we calculate several points of the photoemission spectroscopy (PES) along the corresponding eigenvector. At this point, we use the eigenvectors obtained with VASP. These eigenvectors change little from displacement to displacement (less than the frequencies do) and are a good starting point to plot the PES along a given mode. Figure 1 shows the corresponding one dimensional PES for the O-O stretch, the antisymmetric O_2-Ag, and the center-of-mass modes. The vibrational states ν=0, 1 are obtained by solving the one-dimensional (1D) Schrödinger equation for each PES. At this point, the *ab initio* energies are interpolated with a cubic spline (full lines in Fig. 1). The excitation energy of 84.15 meV for the O-O stretch mode is now in

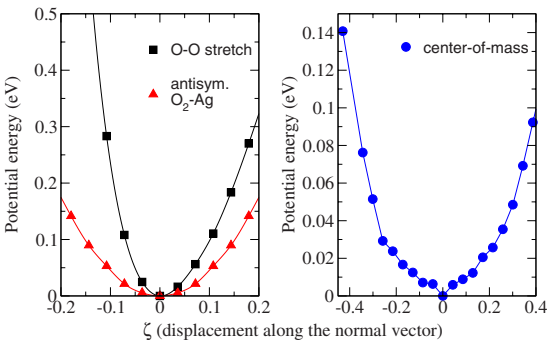

FIG. 1. (Color online) Potential-energy curves of O_2[001] as a function of the displacement along the corresponding normal eigenvector in Å: (a) O-O stretch (squares) and antisymmetric O_2-/Ag (triangles) modes, (b) center-of-mass mode (circles). Lines show the spline interpolation used in each case to solve the 1D Schrödinger equation.

excellent agreement with the experimental data. As shown in the figure, the potential separates from the harmonic behavior quite rapidly. In fact, we have verified that the O-O stretch mode can be perfectly fitted by a Morse potential as in gas phase, what shows the strong molecular character of this mode. In contrast, no much improvement is found for the antisymmetric (48 meV) and, particularly, the center-of-mass (16.07 meV) modes, probably due to using the harmonic approximation in extracting the nuclear displacement for each mode. Therefore, we conclude that the uncertainty in the frequency evaluation is due to the anharmonicities of the PES and not to the DFT calculation.

C. IETS simulations

The IETS simulations of O_2 on Ag(110) consist in calculating the spatial distribution of the conductance changes and the vibrational spectra. For the quantitative evaluation of IETS and its spatial distribution we use the many-body extension of the Tersoff-Hamman theory for the STM.[19,22] The current implementation is based on DFT results regarding the electronic structure and the electron-vibration couplings. Briefly, the conductance change due to the excitation of a localized vibration to the lowest order in the electron-vibration coupling, v, is given by the opening of the inelastic channel, $\Delta\sigma_{ine}(\mathbf{r})$, which leads to an increase in conductance, and the change in the elastic channel to the same order in v, $\Delta\sigma_{ela}(\mathbf{r})$, which means a decrease in conductance. In Ref. 32, an all-order theory shows that the decrease in conductance is related to the appearance of vibrational side bands in the elastic electron transmission. The decrease is maximum when a molecular level is resonant with the Fermi energy and such that side bands appear at $\pm\hbar\Omega$.

Due to the strong molecular character at the Fermi energy, approximations replacing the energy dependence by the behavior at the Fermi energy are not correct any longer. Hence, we use the full electronic structure and energy dependence for the finite bias of the measurements. In this case, we extend the customary IETS treatment[19,22] to new equations that keep all the energetic dependence. Hence, the inelastic contribution to the conductance change is given by

$$\frac{\Delta\sigma_{ine}}{\sigma} = \frac{1}{\rho(\mathbf{r}_0, E_F + eV)} \times \sum_{n,\mathbf{k}} \left| \sum_m \frac{\langle \psi_{m,\mathbf{k}} | v | \psi_{n,\mathbf{k}} \rangle \psi_{m,\mathbf{k}}(\mathbf{r}_0)}{\epsilon_{n,\mathbf{k}} - \epsilon_{m,\mathbf{k}} + i0^+} \right|^2 \times [1 - f(\epsilon_{n,\mathbf{k}})] \delta(E_F + eV - \hbar\Omega - \epsilon_{n,\mathbf{k}}), \quad (1)$$

where $\rho(\mathbf{r}_0, E_F + eV)$ is the local density of states evaluated at the STM tip's center $\mathbf{r}_0$ and at the Fermi energy plus the energy of the electron at the corresponding bias, V. The Fermi distribution function is given by $f(\epsilon)$ and Ω is the frequency of the considered mode. Since we are using periodic-boundary calculations, the electronic states are Bloch states with band indexes n and m and k-vector $\mathbf{k}$. Note that the local electron-vibration potential v couples states with the same k vector. The elastic term is

$$\frac{\Delta\sigma_{ela}}{\sigma} = \frac{-2\pi^2}{\rho(\mathbf{r}_0, E_F + eV)} \sum_{n,\mathbf{k}} \left| \sum_m [1 - f(\epsilon_{m,\mathbf{k}})] \times \langle \psi_{m,\mathbf{k}} | v | \psi_{n,\mathbf{k}} \rangle \psi_{m,\mathbf{k}}(\mathbf{r}_0) \delta(\epsilon_{m,\mathbf{k}} - \hbar\Omega - \epsilon_{n,\mathbf{k}}) \right|^2 \times [1 - f(\epsilon_{n,\mathbf{k}})] \delta(E_F + eV - \hbar\Omega - \epsilon_{n,\mathbf{k}}). \quad (2)$$

The factor $[1-f(\epsilon_{n,\mathbf{k}})]\delta(E_F+eV-\hbar\Omega-\epsilon_{n,\mathbf{k}})$ is responsible for the temperature-dependent onset of the vibrational signal. Indeed, if $eV<\hbar\Omega$, this factor is strictly zero at zero temperature. In the evaluation of these equations the k-point sampling is critical because a large number of electronic states are needed to ensure numerical accuracy. The δ functions are approximated by Gaussian functions of broadening smaller than the used bias. Typically, we have performed the simulations at $V=150$ mV with a Gaussian broadening of 50 meV, except for the O-O stretch mode that is calculated at $V=200$ meV. The requirement being that the broadening be smaller than the used bias but larger than the electronic level spacing due to the discrete k-point sampling. Hence, dense k-point samplings are mandatory for accurate calculations. The experimental change in conductance is simulated as the sum of the inelastic and elastic contributions.

The electron-vibration matrix elements are computed with finite differences using the harmonic approximation.[22,33] In the above calculation of the frequencies and normal modes, we have seen that the harmonic approximation leads to sizeable errors in the estimation of these quantities. However, the inelastic signal is more robust. Indeed, if η is the square-root mean displacement along the normal mode given by $\eta = \sqrt{\hbar/2m\Omega}$ with m some reduced mass, then

$$\frac{\Delta\sigma}{\sigma} \propto \eta^2.$$

We see that an error in η propagates as $1/\eta^3$ in the evaluation of Ω, however the propagation in $\frac{\Delta\sigma}{\sigma}$ is just linear. Hence, small values of η lead to large error bars in the determination of the frequency while the inelastic change in conductance still has reasonable values.

Following Ref. 32, the bias dependence of the inelastic signal is calculated with the SCBA (Refs. 34–37) based on a parametrized Hamiltonian. In spite of the Hamiltonian simplification, SCBA is numerically difficult and the evaluation of the spatial distribution of the SCBA signal is beyond our capabilities. Instead, we have fixed the STM-substrate symmetry and evaluated the IETS as a function of the applied bias. Results are shown depending on temperature and modulation voltage of the experimental lock-in amplifier in Sec. V.

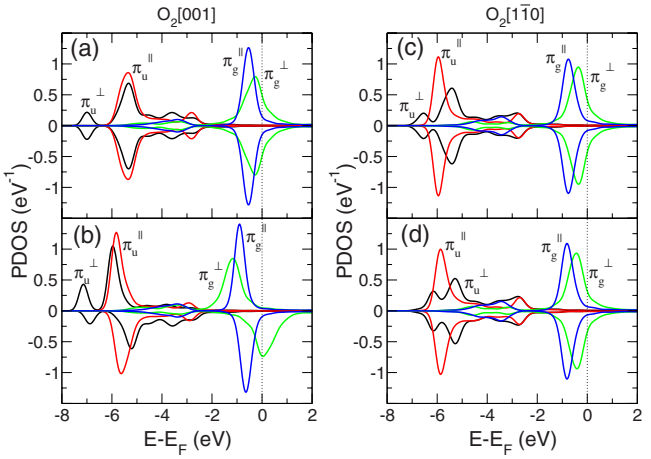

FIG. 2. (Color online) Spin-up (positive) and spin-down (negative) projected density of states of $O_2[001]$ (left panels) and $O_2[1\bar{1}0]$ (right panels) onto the O_2 molecular orbitals. [(a) and (c)] Semilocal DFT (GGA) results. [(b)and (d)] Semilocal DFT+U (GGA+U, $U=3$ eV) results. Intra-atomic correlation leads to a change in the π_g resonance for the $O_2[001]$ only. The Gaussian broadening used in the projections is 0.25 eV.

III. ELECTRONIC STRUCTURE OF O_2 ON Ag(110)

Despite local and semilocal DFT have proven to be accurate in determining variational ground-state properties of the many-body system such as the electron density, it cannot assure a reliable treatment of the spectroscopic properties. In many cases, the electronic structure is incorrect due to the inadequate description of the on-site Coulomb interaction that favors fractional occupancies of energetically close states. This is precisely what happens with the electronic structure of the $O_2[001]$ chemisorption state calculated with GGA. In Fig. 2(a) the projection of the density of states (PDOS) on to the O_2 molecular orbitals (MOs) reflects the partial occupation of the four π_g orbitals, despite the adsorbed molecule is capturing less than two electrons. These unrealistic populations are possibly at the origin of the discrepancy between the experimental IETS and the GGA-based simulations. To solve this failure we have performed DFT+U calculations of O_2 chemisorbed on Ag(110). The DFT+U is aimed to correct the electronic structure without perturbing the physical magnitudes for which the GGA excels. A detail comparison of these quantities is shown in Table II for the two chemisorption states. The good agreement obtained with the GGA values ensures the correct description of the system.

The more realistic DFT+U electronic structure shows that the paramagnetic nature of O_2 is partially preserved when chemisorbed along the [001] direction. As shown in Fig. 2(b), the adequate description of the intramolecular Coulomb

TABLE II. Semilocal DFT (GGA) and DFT+U (GGA+U with U=3 eV) quantities describing the physical properties of the two chemisorption states of O_2 on Ag(110).

	O-O (Å)		O-Ag (Å)		O_2 surface (Å)		Magnetization(μ_B)	
State	GGA	GGA+U	GGA	GGA+U	GGA	GGA+U	GGA	GGA+U
$O_2[001]$	1.43	1.41	2.35	2.37	1.34	1.34	0.0	0.54
$O_2[1\bar{1}0]$	1.45	1.48	2.36	2.35	1.12	1.12	0.0	0.0

interaction breaks the spin degeneracy imposed by GGA and allows the full occupation of the two parallel-to-the-surface π_g orbitals ($\pi_g^{\parallel}$) and the spin-up perpendicular-to-the-surface $\pi_g(\pi_g^{\perp})$. Still the spin-down $\pi_g^{\perp}$ is partially occupied in order to preserve the correct electron density ascribed to the molecule. As a result, this molecular orbital is at resonance with the Fermi level. The electronic structure of this chemisorption state can be viewed as a Stoner-type process in which the molecule reduces its total energy by splitting the orbitals according to their spin polarization. One becomes completely filled at the expense of the other stabilizing the full system.

In contrast, no spin splitting of the $\pi_g^{\perp}$ orbital is obtained for the $O_2[1\bar{1}0]$ molecule. At first sight there are no significant differences on the structural properties (Table II) and the GGA electronic structures of the two chemisorption states [compare Figs. 2(a) and 2(c)]. These similarities are indeed consistent with the experimental observations of almost identical chemisorption energies[13] and equal probability to find any of the two configurations.[14] However, the small differences found in the GGA calculations already point to a slightly larger charge transfer from the surface to the $O_2[1\bar{1}0]$ molecule, which is also closer to the surface and more stretched.[38] Similar results were also found in Ref. 8 using a 3×2 surface cell. Experimentally, this picture agrees with the existence of two energetically close modes that are attributed to the O-O stretching vibration of the $O_2[1\bar{1}0]$ (79.5 meV) and the $O_2[001]$ (85 meV).[13] Our DFT+U calculations show that the induced density for $O_2[1\bar{1}0]$ is larger and the Coulomb repulsion less important. Interestingly, what the DFT+U results highlight is a new difference between the two chemisorption states, namely, the paramagnetic character that is *only* preserved in the $O_2[001]$ molecule.

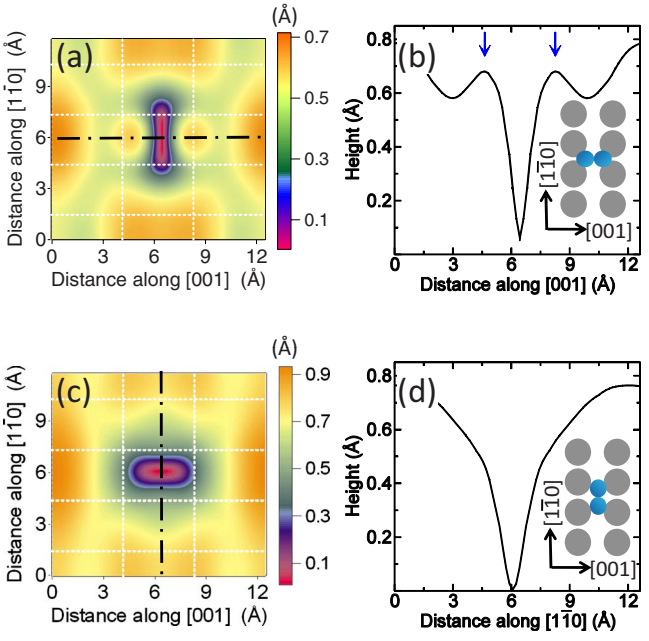

FIG. 3. (Color online) Calculated GGA+U (U=3 eV) local DOS for O_2 on Ag(110) calculated with a sample bias V =200 mV. The zero height corresponds to a tip-surface distance of ~6 Å. [(a) and (b)] Topographical image and profile (both in Å) along the molecular axis for $O_2[001]$. The protrusions attributed to the $\pi_g^{\perp}$ orbital are indicated by arrows. [(c) and (d)] Topographic image and profile (both in Å) along the molecular axis for $O_2[1\bar{1}0]$. The white grid lines in (a) and (c) show the surface structure. The black dashed-dotted lines indicate the direction along the O_2 internuclear axis for each adsorption state.

The DFT+U electronic structures are used to generate the constant current simulations of Fig. 3. The experimental topographical images of the $O_2[001]$ (Ref. 14) and the $O_2[1\bar{1}0]$ (Ref. 15) are well reproduced in both cases. The main difference between both states is the two protrusions appearing along the molecular axis in the former but not in the latter. As was demonstrated by the nonspin-polarized DFT calculations of Olsson *et al.*,[39] these protrusions are the fingerprints of the $\pi_g^{\perp}$ orbital. The absence of these features in the LDOS image of the $O_2[1\bar{1}0]$ molecule is also understood on the basis of the stronger screening exerted on this molecule by the surface electrons. Note, finally, that the similar STM simulations obtained with nonspin-polarized DFT and spin-polarized DFT+U show that information about the spin moment cannot be directly extracted from the STM topography. In the next section, we will see that STM-based IETS can alternatively be used to identify this peculiar electronic structure in which a spin-polarized MO is at resonance with the Fermi level.

The particular electronic structure of O_2 on the surface is strongly dependent on the nature of the surface itself. A more reactive surface such as a copper one would lead to stronger hybridization with the molecule and to a larger charge transfer, pulling the π_g resonance completely below the Fermi energy.[40] For a copper surface, the mixed-valence regime described above is not possible.

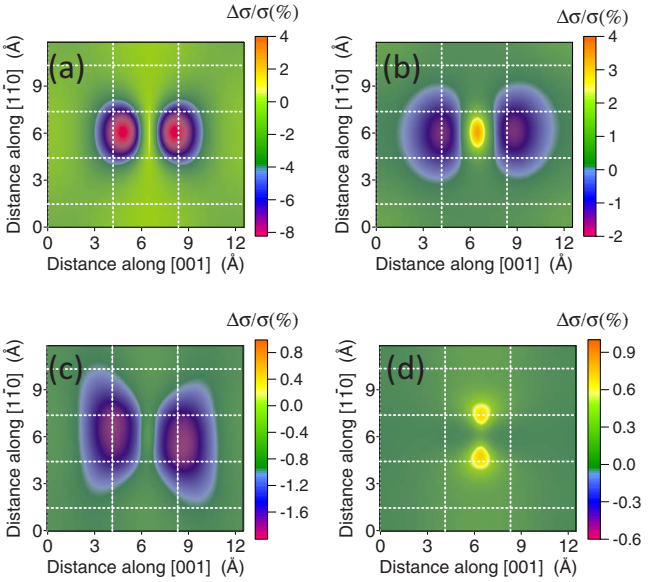

FIG. 4. (Color online) Calculated GGA+U (U=3 eV) STM-IETS for O_2 chemisorbed on Ag(110) along the [001] direction. Spatial distribution of the conductance changes for (a) the symmetric O-O stretch mode, (b) the antisymmetric O_2-Ag stretch mode, (c) the center-of-mass or symmetric O_2-Ag stretch mode, and (d) the hindered rotation mode. Note the negative and positive conductance changes observed on the antisymmetric mode, in contrast to the overall negative values of the O-O stretch and center-of-mass modes or the positive values of the hindered rotation one. The white grid lines show the Ag (110) surface structure.

IV. SPATIAL DISTRIBUTION OF CONSTANT CURRENT IETS SIGNALS

Our STM-IETS simulations, based on the DFT+U electronic structure, are able to reproduce qualitatively, and many times quantitatively, the reported experimental findings: (i) the negative conductance changes observed in the vibrational spectra of the O_2[001] molecule, (ii) the spatial distribution of the conductance changes recorded over the O_2[001] molecule for the O-O stretch and the antisymmetric O_2-Ag stretch vibrations, (iii) the absence of signal for the center of mass and hindered rotation modes, and (iv) the lack of IETS signal for the molecule chemisorbed along the [1$\bar{1}$0] direction.[15]

We start by analyzing the spatial distribution of the conductance change for the O_2[001] molecule. A schematic of the vibrational modes is depicted in Fig. 5. Figure 4(a) shows that the symmetrical O-O stretch mode leads to a decrease in conductance over the adsorbed molecule. In agreement with the experiment, the maximum absolute value of conductance change is displaced from the center of the oxygen atoms in the same way as the constant current STM image. This is reminiscent of the $\pi_g^\perp$ orbital, showing that the conductance decrease due to this vibrational mode can be understood within the framework of a single-level resonant with the Fermi energy. Model calculations[18] demonstrated that the presence of a substantial density of states at the Fermi energy of large molecular character leads to an important IETS signal of negative sign, i.e., a reduction in conductance over the vibrational threshold, as observed here.

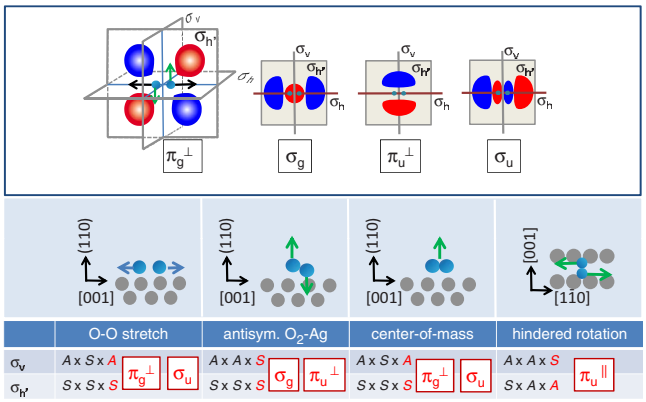

FIG. 5. (Color online) Sketch and symmetries of the MOs and modes involved in the IETS images. The table summarizes the MOs that can couple with the $\pi_g^\perp$ to assure a nonzero matrix element $\langle\psi_{m,\mathbf{k}}|v|\psi_{n,\mathbf{k}}\rangle$ [see Eqs. (1) and (2)]. The symmetric (S) or antisymmetric (A) character of the $\pi_g^\perp$ and the electron-vibration coupling v is written in black following this order for each vibrational mode and symmetry plane. In gray (red), the symmetry character of $\psi_{m,\mathbf{k}}$ necessary for a nonzero coupling. The MOs fulfilling those symmetry conditions are written inside the gray (red) squares.

The antisymmetric stretch mode is more interesting. Here, the oxygen atoms move vertical to the surface with opposite phases. Again, in good agreement with the experiment, we find that while the change in conductance is negative away from the molecular center, it is positive at the molecular center [Fig. 4(b)]. In contrast to the O-O stretch mode, this behavior implies that the IETS signal involves the coupling with various molecular orbitals and, therefore, we should go beyond the single-level model to understand this IETS image.

Simulations performed for the center-of-mass mode show a negative conductance change image rather similar to the one obtained for the O-O stretch mode, Fig. 4(c). The maximum conductance decrease however is a factor of 5 lower in the center of mass, what explains the absence of signal in the experiments for this mode. The simulated efficiency for the hindered rotation mode, in which the atoms try to move opposite to each other along the [1$\bar{1}$0] surface direction, is even smaller: less than 0.8% of conductance change, Fig. 4(d). Neither is this mode observed in the recorded IETS data.

All the above results can be understood with the help of Eqs. (1) and (2). As the $\pi_g^\perp$ is the only MO at resonance with the Fermi level, the topography of the conductance changes is determined by the molecular-orbitals coupling with such single resonance, i.e., by those MOs contributing with nonzero matrix elements in Eqs. (1) and (2). The symmetry analysis summarized in the table of Fig. 5 provides a schematic idea of the MOs that can couple with the $\pi_g^\perp$ for each vibrational mode. The weight of these couplings in the IETS image will ultimately depend on the orbitals energies and on the strength of the electron-vibration coupling v, as discussed below.

There are two well-defined symmetry planes in this system: the plane perpendicular to the molecular axis σ_v and the

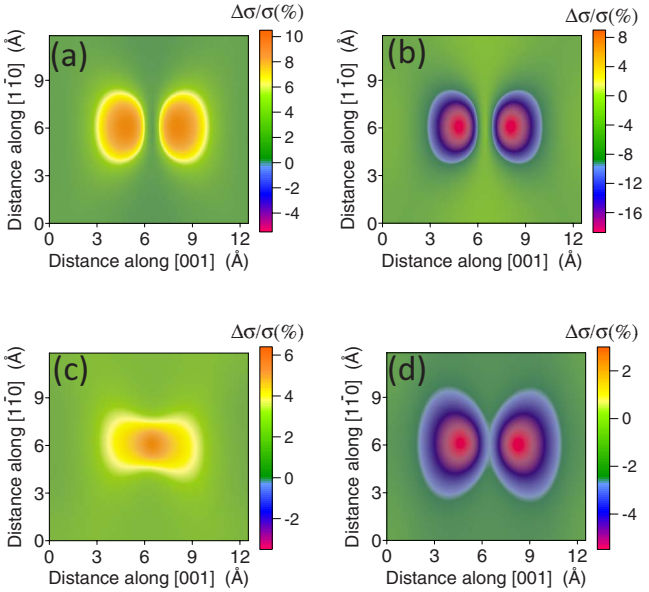

FIG. 6. (Color online) Contributions (in %) to the conductance changes shown in Fig. 4 for O_2[001]. (a) Inelastic and (b) elastic contributions to the O-O stretch mode. (c) Inelastic and (d) elastic to the antisymmetric O_2-Ag stretch mode.

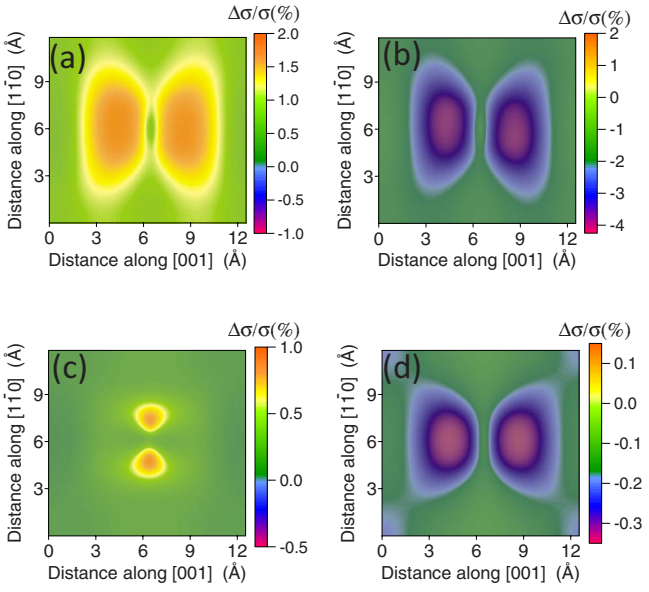

FIG. 7. (Color online) Contributions (in %) to the conductance changes for O_2[001]. (a) Inelastic and (b) elastic contributions for the center-of-mass stretch mode. (c) Inelastic and (d) elastic for the hindered rotation mode.

plane normal to the surface that contains the molecular axis σ_h'. The regions where the wave functions take positive and negative values are schematically depicted for each MO in the upper panel of Fig. 5 with blue and red colors, respectively. As written in the table, the $\pi_g^\perp$ is antisymmetric (A) respect to σ_v and symmetric (S) respect to σ_h'. Since the O-O stretch mode is symmetric respect to both planes, the coupling electronic states should, respectively, be A and S. These conditions are only satisfied by the $\pi_g^\perp$ and the σ_u orbitals. The same conclusion is obtained for the center-of-mass mode, which is also symmetric respect to both planes. The A and S characters of the antisymmetric O_2-Ag stretch mode respect to σ_v and σ_h', force the coupling of $\pi_g^\perp$ with the σ_g and the $\pi_u^\perp$ orbitals. Finally, the excitation of the hindered rotation mode, which presents a fully antisymmetric character, couples the $\pi_g^\perp$ with the $\pi_u^\parallel$ orbital only.

Once we know which orbitals are coupled by each vibrational mode, the topography of the IETS signal is better understood if the conductance change is divided in its inelastic contribution due to the opening of a new channel, hence positive, and the renormalization of the elastic channel due to the presence of the vibration that leads to a negative contribution. Figures 6 and 7 show the inelastic (left panels) and elastic (right panels) contributions for the four vibrational modes. According to Eqs. (1) and (2), the main difference between them despite their sign, is that the inelastic part involves all possible intermediate electronic states, while the states contributing to the elastic part are restricted by the extra δ function to an energy interval on the order of the mode frequency $\hbar\Omega$ about the Fermi energy. This strict energy restriction explains that in all cases the $\pi_g^\perp$, being the only orbital at resonance with the Fermi level, dominates the topography of the elastic contribution.

In contrast, the inelastic image can be composed by all the coupling states that according to the symmetry analysis contribute with nonzero matrix elements in Eq. (1). The weight of each coupling state in the IETS image is partially determined by the denominator of Eq. (1), penalizing the orbitals that are energetically distant from E_F. The effect of the different weighing is reflected in the simulations of the inelastic contributions. Figures 6(a) and 7(a) show that the inelastic contribution is due to the $\pi_g^\perp$ (at resonance with E_F) and not to the energetically distant σ_u in the O-O stretch and center-of-mass modes. Otherwise, there would be a certain intensity modulation along the molecular axis caused by the nodes of the σ_u orbital. Similarly, the absence of nodes along the molecular axis and the maximum intensity obtained at the center of the molecule in Fig. 6(c) show that the image is basically due to the $\pi_u^\perp$ and not to the σ_g in the antisymmetric stretch mode. In the hindered rotation mode, Fig. 7(c) shows that the inelastic contribution is uniquely formed by the $\pi_u^\parallel$ as predicted by the previous symmetry analysis.

Now, we have all the ingredients necessary to understand the IETS data recorded for the O_2[001] molecule. In the O-O stretch mode, the elastic and inelastic contributions are only due to the $\pi_g^\perp$ orbital. As the elastic part is much larger than the inelastic one, the excitation of this vibration leads to an overall reduction in conduction except between the O atoms where the π_g orbital presents a nodal plane. Compared with the O-O stretch mode, the smaller elastic and inelastic contributions obtained in the center-of-mass mode are due to the weaker electron-phonon coupling, as can be roughly inferred from the different vibrational energy of each mode (see Table I). In consequence, no IETS signal is observed in the center-of-mass mode, despite its symmetry similarities with the O-O stretch mode. The antisymmetric O_2-Ag mode is more complex because involve different orbitals: the inelastic part is dominated by $\pi_u^\perp$ and the elastic part by the $\pi_g^\perp$. The rich structure observed in this mode is a consequence of the different nodal structure of the two orbitals. The total conduc-

tance change is positive in the region between the two oxygen atoms because the elastic contribution is zero whereas the inelastic one is maximal. On the contrary, the conductance change is negative out of the internuclear region because there the elastic part is maximal and the inelastic part minimal. Finally, the absence of IETS signal for the hindered rotation mode is a consequence of two factors: the low DOS with $\pi_u^{\parallel}$ character around E_F and the weak electron-phonon coupling of this mode.

We also perform simulations of the conductance changes for the $O_2[1\bar{1}0]$ chemisorption state. The absence of experimental IETS signal is in agreement with our calculations that show changes of about 1% at most. The reason behind this small changes in conductance is due to the almost complete occupancy of $\pi_g^{\perp}$ that renders very small the probability to excite any vibrational mode by tunneling trough this MO.

V. BIAS DEPENDENCE OF IETS: A SELF-CONSISTENT BORN APPROXIMATION STUDY

In order to compute the bias dependence of the inelastic signal, we use the SCBA. Briefly, the SCBA consists in using the Born expression for the electron-vibration self-energy (lowest order in the electron-vibration matrix element) replacing the free-electron Green's function by the full Green's function.[41] This last function is unknown, hence an iterative process is used where the starting step is the free-electron Green's function, and the second step uses the self-energy computed with the Green's function obtained from the first step. This self-consistent procedure is stable and has the virtue of generating high-order terms in the electron-vibration coupling.

The SCBA has been implemented in DFT-based approaches[42] but it is a costly method for evaluating STM scans as the ones shown herein. It is however feasible for a single STM conformation, where the bias is ramped and a d^2I/dV^2 spectrum is obtained. Here, we have simplified the problem and taken the tight-binding parametrization of Ref. 32. Namely, a single orbital at the Fermi energy, with a broadening, $\Gamma=0.4$ eV, an electron-vibration matrix element, $M=0.04$ eV, and the stretch frequency of 0.08 eV. As we have seen, the excitation of the antisymmetric O_2-Ag stretch mode is a truly multiorbital problem, and we cannot apply this simple model to compute the dI/dV for this mode. Moreover, in Ref. 32 it was shown that molecular modes can have non-negligible interactions through the electron-vibration coupling leading to a shifting of the actual vibrational thresholds. The SCBA can be performed for multiorbital and multimode problems such as the vibration excitation of C_{60} of Ref. 43, however, here our aim is to show the vibrational line shape to be expected in the d^2I/dV^2 spectrum of the stretch mode and how it is distorted by the presence of thermal effects and bias modulation.

As discussed in Ref. 44, the SCBA fails in the limit of large electron-vibration coupling. The main reason is because the SCBA fails in taking into account the correct contribution of the number of excited modes. Indeed, Ness[44] shows that SCBA yields the same result as an exact calculation if the electron-vibration matrix elements did not depend on the number of excited modes. If the average number of excited modes is on the order of 1, then the SCBA gives a very good account of the vibrational excitation even in the case of extraordinary vibronic effects.[43] Approaches going beyond SCBA are available[45,46] and are necessary for exploring realistic situations where the electron-vibration coupling is strong enough to excite several overtones.

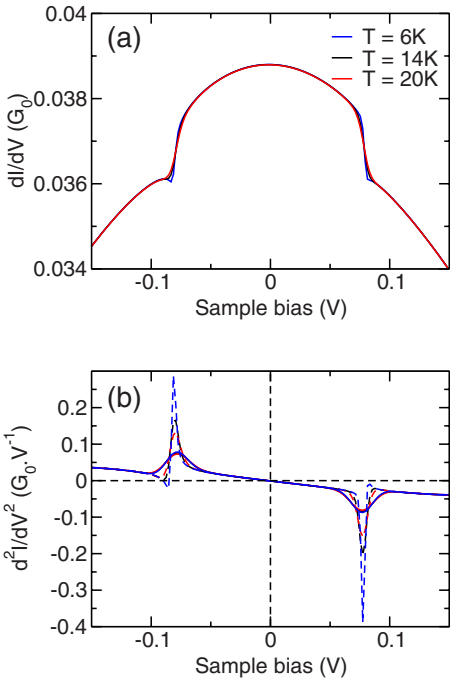

FIG. 8. (Color online) (a) Conductance of O_2 on Ag (110) along the [001] direction in a model tunnel junction. The O-O stretch mode is allowed to interact with the tunneling electrons leading to a decrease in conductance over the vibrational threshold. (b) Derivative of the conductance with respect to the applied bias. Both graphs show the behavior with temperature. In (b) the full line spectra have been convoluted with a Gaussian broadening representing the effect of a 7 mV rms modulation voltage. Results shown in (a) and dashed lines in (b) are without modulation-voltage broadening.

Figure 8 shows the results of the SCBA for the O-O stretch mode. Panel (a) shows the conductance, mainly given by the molecular resonance about the Fermi energy, and two sharp Stokes and anti-Stokes changes in conductance. In (b) the conductance derivative or d^2I/dV^2 is shown. In both cases three different temperatures are used, 6, 14, and 20 K. At low temperatures the d^2I/dV^2 shows a Fano profile as has already been discussed for the excitation of vibrations by electronic currents,[34] however as the temperature increases, the peak becomes broadened and closer to a simple Lorentzian peak. It is the modulation voltage used in the lock-in detection that finally broadens and removes any particular detail from the excitation peak. Figure 8(b) shows in full line the peaks after convolution[47] using a modulation voltage of 7 mV rms as in the experiment.[14]

VI. CONCLUSIONS

We have conducted STM-IETS simulations based on the DFT+U electronic structure and applying an extension of

the Tersoff-Hamman theory to the presence of inelastic effects.[19,22] Our results are able to reproduce the experimental IETS recorded by Hahn *et al.*:[14,15] (i) the negative conductance changes observed in the vibrational spectra of the O_2[001] molecule, (ii) the spatial distribution of the conductance changes recorded over the O_2[001] molecule for the O-O stretch and the antisymmetric O_2-Ag stretch vibrations, (iii) the absence of signal for the center of mass and hindered rotation modes, and (iv) the lack of IETS signal for the molecule chemisorbed along the $[1\bar{1}0]$ direction. These results permit us to give an enhanced description of the IETS signals in terms of the molecular symmetries of the adsorbed system. Leading to the conclusion that a multiorbital description is mandatory and that the simulation is able to capture the complex increases and decreases in conductance depending on the STM tip location over the molecule.

The good agreement of the simulations with the experiment validates the results of the electronic structure as computed with DFT+U. In particular, DFT+U shows that out of the two possible molecular conformations on the surface, only the one along the [001] direction is paramagnetic.

The inclusion of the U correction does not alter the values of the other DFT parameters such as the molecular geometry and vibrational structure. Regarding vibrations, in order to attain reliable numerical values of the molecular frequencies, we have used a Morse potential to fit the DFT potential-energy surface because anharmonicities rapidly set in and good frequency values are difficult to obtain.

Finally, Fano-type profiles are revealed for the IETS as a function of the bias voltage, however the two main sources of experimental broadening (temperature and more importantly the lock-in modulation voltage) erases any information of the actual spectral line shapes.

ACKNOWLEDGMENTS

We acknowledge financial support from the Spanish MICINN (Grants No. FIS2007-066711-CO2-00 and No. FIS2009-12721-C04-01), and the Basque Government-UPV/EHU (Grant No. IT-366-07). Computational resources were provided by the Centre de Calcul de Midi-Pyrénées, the DIPC and the SGI/IZO-SGIker.

[1] B. C. Stipe, M. A. Rezai, and W. Ho, Science **280**, 1732 (1998).
[2] W. Ho, J. Chem. Phys. **117**, 11033 (2002).
[3] T. Komeda, Prog. Surf. Sci. **78**, 41 (2005).
[4] N. Okabayashi, Y. Konda, and T. Komeda, Phys. Rev. Lett. **100**, 217801 (2008).
[5] H. Gawronski, M. Mehlhorn, and K. Morgenstern, Science **319**, 930 (2008).
[6] B. C. Stipe, M. A. Rezaei, W. Ho, S. Gao, M. Persson, and B. I. Lundqvist, Phys. Rev. Lett. **78**, 4410 (1997).
[7] M. Ohara, Y. Kim, S. Yanagisawa, Y. Morikawa, and M. Kawai, Phys. Rev. Lett. **100**, 136104 (2008).
[8] P. A. Gravil, D. M. Bird, and J. A. White, Phys. Rev. Lett. **77**, 3933 (1996).
[9] M. Alducin, H. F. Busnengo, and R. Díaz-Muiño, J. Chem. Phys. **129**, 224702 (2008).
[10] L. Vattuone, C. Boragno, M. Pupo, P. Restelli, M. Rocca, and U. Valbusa, Phys. Rev. Lett. **72**, 510 (1994).
[11] A. Raukema, D. A. Butler, F. M. A. Box, and A. W. Kleyn, Surf. Sci. **347**, 151 (1996).
[12] F. Buatier de Mongeot, M. Rocca, and U. Valbusa, Surf. Sci. **363**, 68 (1996).
[13] F. Bartolucci, R. Franchy, J. C. Barnard, and R. E. Palmer, Phys. Rev. Lett. **80**, 5224 (1998).
[14] J. R. Hahn, H. J. Lee, and W. Ho, Phys. Rev. Lett. **85**, 1914 (2000).
[15] J. R. Hahn and W. Ho, Phys. Rev. Lett. **87**, 196102 (2001).
[16] J. R. Hahn and W. Ho, J. Chem. Phys. **122**, 244704 (2005); **123**, 214702 (2005).
[17] M. Alducin, D. Sánchez-Portal, A. Arnau, and N. Lorente, Phys. Rev. Lett. **104**, 136101 (2010).
[18] B. N. J. Persson and A. Baratoff, Phys. Rev. Lett. **59**, 339 (1987).
[19] N. Lorente and M. Persson, Phys. Rev. Lett. **85**, 2997 (2000).
[20] M. Paulsson, T. Frederiksen, H. Ueba, N. Lorente, and M. Brandbyge, Phys. Rev. Lett. **100**, 226604 (2008).
[21] O. Tal, M. Krieger, B. Leerink, and J. M. van Ruitenbeek, Phys. Rev. Lett. **100**, 196804 (2008).
[22] N. Lorente, Appl. Phys. A **78**, 799 (2004).
[23] A. C. Hewson, *The Kondo Problem to Heavy Fermions* (Cambridge University Press, Cambridge, 1993).
[24] G. Kresse and J. Hafner, Phys. Rev. B **47**, 558 (1993); **48**, 13115 (1993); G. Kresse and J. Furthmüller, Comput. Mater. Sci. **6**, 15 (1996); Phys. Rev. B **54**, 11169 (1996).
[25] G. Kresse and D. Joubert, Phys. Rev. B **59**, 1758 (1999).
[26] J. P. Perdew, J. A. Chevary, S. H. Vosko, K. A. Jackson, M. R. Pederson, D. J. Singh, and C. Fiolhais, Phys. Rev. B **46**, 6671 (1992).
[27] S. L. Dudarev, G. A. Botton, S. Y. Savrasov, C. J. Humphreys, and A. P. Sutton, Phys. Rev. B **57**, 1505 (1998).
[28] M. Cococcioni and S. de Gironcoli, Phys. Rev. B **71**, 035105 (2005).
[29] B. A. Sexton and R. J. Madix, Chem. Phys. Lett. **76**, 294 (1980).
[30] C. Backx, C. P. M. De Groot, and P. Biloen, Surf. Sci. **104**, 300 (1981).
[31] Richard Martin, *Electronic Structure: Basic Theory and Practical Methods* (Cambridge University Press, Cambridge, 2004).
[32] S. Monturet and N. Lorente, Phys. Rev. B **78**, 035445 (2008).
[33] N. Lorente and M. Persson, Faraday Discuss. **117**, 277 (2000).
[34] M. Galperin, M. A. Ratner, and A. Nitzan, J. Chem. Phys. **121**, 11965 (2004).
[35] T. Frederiksen, M. Brandbyge, N. Lorente, and A.-P. Jauho, Phys. Rev. Lett. **93**, 256601 (2004).
[36] G. C. Solomon, A. Gagliardi, A. Pecchia, T. Frauenheim, A. Di Carlo, J. R. Reimers, and N. S. Hush, J. Chem. Phys. **124**, 094704 (2006).
[37] D. A. Ryndyk, M. Hartung, and G. Cuniberti, Phys. Rev. B **73**, 045420 (2006).

[38] The integration up to E_F of the PDOS corresponding to the π_g orbitals gives values of 1.35e in $O_2[001]$ and 1.8e in the $O_2[1\bar{1}0]$.
[39] F. E. Olsson, N. Lorente, and M. Persson, Surf. Sci. **522**, L27 (2003).
[40] A. Puisto, H. Pitkänen, M. Alatalo, S. Jaatinen, P. Salo, A. S. Foster, T. Kangas, and K. Laasonen, Catal. Today **100**, 403 (2005).
[41] H. Haug and A.-P. Jauho, *Quantum Kinetics in Transport and Optics of Semiconductors* (Springer-Verlag, Berlin, 1996).
[42] J. R. Reimers, G. C. Solomon, A. Gagliardi, A. Bilić, N. S. Hush, T. Frauenheim, A. Di Carlo, and A. Pecchia, J. Phys. Chem. A **111**, 5692 (2007).
[43] T. Frederiksen, K. J. Franke, A. Arnau, G. Schulze, J. I. Pascual, and N. Lorente, Phys. Rev. B **78**, 233401 (2008).
[44] H. Ness, J. Phys.: Condens. Matter **18**, 6307 (2006).
[45] M. Galperin, A. Nitzan, and M. A. Ratner, Phys. Rev. B **73**, 045314 (2006).
[46] R. Härtle, C. Benesch, and M. Thoss, Phys. Rev. Lett. **102**, 146801 (2009).
[47] T. Frederiksen, M. Paulsson, M. Brandbyge, and A.-P. Jauho, Phys. Rev. B **75**, 205413 (2007).